Journal of Fluorescence, Vol. 15, No. 6, December 2005 (© 2005)
DOI: 10.1007/s10895-005-0012-5

High Probe Intensity Photobleaching Measurement of Lateral Diffusion in Cell Membranes

Guy M. Hagen,[1] Deborah A. Roess,[2] Gildardo Cruz de León,[1] and B. George Barisas[1,3]

Received July 12, 2005; accepted September 8, 2005
Published online: November 29, 2005

Lateral diffusion measurements, most commonly accomplished through Fluorescence Photobleaching Recovery (FPR or FRAP), provide important information on cell membrane molecules' size, environment and participation in intermolecular interactions. However, serious difficulties arise when these techniques are applied to weakly expressed proteins of either of two types: fusions of membrane receptors with visible fluorescent proteins or membrane molecules on autofluorescent cells. To achieve adequate sensitivity in these cases, techniques such as interference fringe FPR are needed. However, in such measurements, cytoplasmic species contribute to the fluorescence recovery signal and thus yield diffusion parameters not properly representing the small number of surface molecules. A new method helps eliminate these difficulties. High Probe Intensity (HPI)-FPR measurements retain the intrinsic confocality of spot measurements to eliminate interference from fluorescent cytoplasmic species. However, HPI-FPR methods lift the previous requirement that FPR procedures be performed at probe beam intensities low enough to not induce bleaching in samples during measurements. The high probe intensities now employed provide much larger fluorescence signals and thus more information on molecular diffusion from each measurement. We report successful measurement of membrane dynamics by this technique.

KEY WORDS: Photobleaching; FPR; FRAP; membrane; green fluorescent protein; diffusion.

INTRODUCTION

Lateral diffusion measurements, most commonly accomplished through Fluorescence Photobleaching Recovery (FPR[4] or FRAP), provide important information on molecules', particularly membrane molecules', size, environment and participation in intermolecular interactions including ligand-driven associations.

FPR measurements on cellular membrane proteins present various challenges. First, many such membrane receptors are expressed at levels as low as 10,000 per cell. Therefore, techniques must be employed which deal with the correspondingly low fluorescence signals. Second, fluorescent species in the cytoplasm, such as visible fluorescent protein (VFP) constructs undergoing transport to the membrane or autofluorescent cytoplasmic compounds, are frequently present in cells to be examined. These cytoplasmic molecules contribute to the fluorescence recovery signal and thus distort measurements aimed at surface molecules. Thus, FPR methods are required which examine cell membrane molecules without interference from cytoplasmic species.

[1] Department of Chemistry, Colorado State University, Fort Collins, Colorado
[2] Department of Biomedical Sciences, Colorado State University, Fort Collins, Colorado
[3] To whom correspondence should be addressed. E-mail: barisas@lamar.colostate.edu

[4] *Abbreviations:* 2H3, rat basophilic leukemia cells of the 2H3 cell line; CHO, Chinese hamster ovary; D, diffusion coefficient; DMEM, Dulbecco's modified Eagle medium; erbB1, receptor tyrosine kinase also known as epidermal growth factor receptor; FITC, fluorescein isothiocyanate; FPR (or FRAP), fluorescence photobleaching recovery; GFP, enhanced green fluorescent protein; HCG, human chorionic gonadotropin; HPI, high probe intensity; IF, interference fringe; LH(R), luteinizing hormone (receptor); *M*, fractional mobility; MEM, minimal essential medium; NA, numerical aperture; TIR, total internal reflection; VFP, visible fluorescent protein.

1053-0509/05/1200-0873/0 © 2005 Springer Science+Business Media, Inc.

The common method of spot FPR [1] using a tightly focused laser beam is easy to implement and the confocality conferred by the image plane aperture substantially eliminates cytoplasmic fluorescence. However, the fluorescence signal obtainable from a sub-micrometer membrane spot is typically small, especially given low levels of receptor expression, and signal-to-noise ratios of individual fluorescence recovery traces are correspondingly low. Thus large numbers of individual measurements typically must be averaged to yield acceptable results.

To avoid this difficulty, we previously developed Interference Fringe Fluorescence Photobleaching Recovery (IF-FPR) [2] to permit simultaneous interrogation of a cell's entire surface. In this method, a three-dimensional fringe pattern is generated interferometrically within the optical path of an FPR system by intersecting two laser beams at the rear image plane of the objective. The fringe pattern interrogates the entire cell at once and so affords much increased signal levels and greatly improved reproducibility of measurements. However, the technique intrinsically possesses tremendous depth of field and so collects fluorescence from the entire cell volume. Hence, it is not satisfactory for cells expressing green fluorescent protein (GFP) fusion proteins or other cells with high levels of cytoplasmic fluorescence. Total Internal Reflection (TIR) [3] allows selective excitation of fluorophores contacting a glass–water interface since the evanescent wave decays exponentially above the interface with a decay length on the order of 100 nm. We have previously combined objective-type TIR illumination with interferometric fringe generation to selectively measure lateral diffusion of only membrane species on living cells [4].

Spot FPR methods allow a different strategy for improving quality of data obtained. In such experiments investigators frequently increase the intensity of the probe laser beam in an effort to improve signal levels. However, photobleaching by the probe beam during such measurements distorts the recovery kinetics in complex ways that have, in the past, not fully been appreciated. This distortion makes accurate estimates of the diffusion coefficient and fractional mobility impossible when data are acquired and analyzed by standard techniques [1]. This problem has been encountered recently in a multiphoton-FPR experiment on microinjected spiny dendrites of cerebellar purkinje cells [5], where some data were discarded due to excessive photobleaching in the probe beam. We have now developed a method, a preliminary description of which has appeared previously [4], which we term High Probe Intensity Fluorescence Photobleaching Recovery (HPI-FPR) and in which we increase the probe beam power up to 10-fold over that typically used. We thus obtain substantially more data per unit time from the illuminated region which remains the same as in spot FPR. This higher probe power causes marked sample photobleaching during recovery. Nonetheless, by acquiring data from the absolute beginning of sample exposure to the probe beam and analyzing these data as described below, accurate values for diffusion parameters are obtained with precision improved substantially over conventional spot methods.

EXPERIMENTAL METHODS

Materials

Minimal essential medium (MEM), Dulbecco's modified Eagle medium (DMEM) containing high glucose, geneticin, cell culture antibiotic solutions, and fetal bovine serum (FBS) were all purchased from Invitrogen, Carlsbad, CA. Non-essential amino acids were purchased from Sigma Chemical Co., St Louis, MO. Alexa 488 was purchased from Molecular Probes, Eugene, OR. G63 MAFA-specific mAb was a kind gift of Professor Israel Pecht, Weizmann Institute of Science, Rehovot, Israel.

Cell Lines and Sample Preparation

Chinese hamster ovary (CHO) cells were stably transfected with C-terminal fusion proteins of enhanced GFP with wild-type rat luteinizing hormone receptor (GFP-LHR cells) [6] and maintained in DMEM with high glucose containing 10% fetal bovine serum, antibiotics and non-essential amino acids, pH 7.4, supplemented with 200 μg/mL geneticin to select for cells expressing GFP fusion proteins. Rat basophilic leukemia cells of the 2H3 line (2H3 cells) were maintained in MEM supplemented with antibiotics and 15% FBS. All cells were grown at 100% humidity in 5% CO_2 at 37°C. After removal from tissue culture flasks using 5 mM EDTA in PBS, cells were pelleted at 300x $\times$ g and re-suspended in PBS. In some experiments, 2H3 cells were labeled with Alexa 488 conjugates of G63 Fab as described previously [7]. Cells were placed on well slides, overlaid with No. 1.5 Pyrex coverslips and then inverted on the microscope. No fixation or mounting agents were used and measurements were performed out at room temperature.

Fluorescence Photobleaching Recovery Measurements

The optical system for fluorescence photobleaching recovery measurements has been described in detail [2]. The inverted Zeiss Axiomat microscope used in this study was equipped with a Zeiss 63 $\times$ Plan Neofluar water immersion objective, NA 1.2. An attenuated Coherent Radi-

ation Innova 100 argon ion laser operating at 488 nm was focused to a spot of 0.38 μm e^{-2} radius and a standard Zeiss FITC-selective filter set was used for both Alexa 488 and GFP fluorophores. In conventional spot photobleaching measurements, bleaching beam power was typically 6 mW. For HPI-FPR measurements, powers were approximately 5- to 10-fold higher. The ratio of intensities in the bleaching and probe beams was held constant at about 3000 and was measured carefully for HPI measurements. A confocal image plane photometer aperture was used in both conventional spot and HPI-FPR spot measurements to eliminate out-of-plane fluorescence. HPI-FPR measurements required that the sample be illuminated with the probe laser beam only during data acquisition. To permit accurate focusing on the sample, a 3 mW 635 nm diode laser (Coherent Auburn Division, Auburn, CA) was aligned co-linear with the optical axis. Objective focus at the level of the cell membrane was detected by the appearance of a sharp spot of scattered red light. This laser was turned off at the beginning of data acquisition. For all experiments, data were acquired at 50 ms/point for 20 s before and for 25 s after the bleaching pulse and were processed off-line with a Marquardt non-linear curve fitting program developed for this application. Conventional spot photobleaching data were analyzed assuming no bleaching by the probe beam while HPI-FPR data were analyzed to allow a non-zero rate of probe bleaching. In some instances, the ratio of bleach and probe intensities and the length of the bleach pulse were input into the fitting procedure to fix the relation between the rate of probe bleaching and the extent of bleaching by the bleaching pulse. This strategy reduced the number of fitted quantities by one and, hence, improved the precision of other fitted parameters. For curve fitting purposes, fluorescence recovery curves were calculated either from the series solution, or from direct numerical simulation, of the bleaching–diffusion equation as described below. Analysis of each recovery trace yielded the initial fluorescence, the rate constant for bleaching in the probe beam (set to zero for conventional spot data), the extent K of bleaching in the bleach pulse [1], the diffusion coefficient and the fraction of fluorescent molecules mobile on the experimental timescale, as well as linear estimates of uncertainties in these quantities. Average values for parameters obtained from replicate measurements are presented $\pm$ the standard deviation of the replicate values.

THEORY UNDERLYING ANALYSIS OF HPI-FPR DATA

Efficient calculation of diffusion accompanied by continuous bleaching is not a trivial problem. The corresponding differential equation does not represent a standard problem in heat conduction and so has not benefitted from the extensive attention historically accorded such topics. A number of other investigators have examined various aspects of continuous photobleaching [8–11], but the specific issue of obtaining accurate diffusion parameters from pulse photobleaching data where the probe beam causes substantial bleaching does not seem to have been addressed adequately. For isotropic diffusion of a single species accompanied by bleaching by a radially symmetric beam, the diffusion equation is

$$D\nabla^2 c(r,t) - BI(r,t)c(r,t) = \frac{\partial c(r,t)}{\partial t} \tag{1}$$

where $c(r, t)$ is the fluorophore concentration, D is the diffusion coefficient, $I = I(r, t)$ is the light intensity and B is the rate-constant for bleaching by light of unit intensity. Assuming the light beam to possess a constant Gaussian radial profile, we may replace $I(r, t)$ with $\exp(-2r^2/r_0^2)\, I(t)$ and, substituting g^2 for $2/r_0^2$, rearrange the equation to read

$$D\nabla^2 c - \frac{\partial c}{\partial t} = Be^{-g^2r^2} I(t)\, c \tag{2}$$

Calculation of probe bleaching effects on Gaussian spot photobleaching data can be approached in various ways. We consider two particular strategies with differing ranges of applicability and levels of sophistication.

Approach 1: Power series solution of differential equation for coupled diffusion and bleaching in a Gaussian beam.

We assert the existence of a power series solution in B for the inhomogeneous partial differential equation, Eq. (2) [12]. Without loss of generality, the first term of this series may be taken to be unity. Further, B can be arbitrarily partitioned into the product of two constants B' and B'', either of which may be taken to be the power series variable.

$$c = 1 + \sum_{n=1}^{\infty} B^n c_n' = 1 + \sum_{n=1}^{\infty} (B'B'')^n c_n' \tag{3}$$

Equating like powers of B', and then setting B'' equal to B, we obtain a series of functions

$$c = 1 + \sum_{n=1}^{\infty} c_n \tag{4}$$

for which the recursion relation is

$$D\nabla^2 c_n - \frac{\partial c_n}{\partial t} = e^{-g^2r^2} BI(t) c_{n-1} \tag{5}$$

The c in Eq. (4) then converges for all $BI(t)$. We assert that each c_n exists as a Bessel Fourier transform:

$$c_n = \int_{k=0}^{\infty} a_n(k,t) J_0(kr) k dk \tag{6}$$

Since Bessel functions are Eigenfunctions of the Laplacian in radial coordinates, we combine Eqs. (5) and (6) to obtain

$$\begin{aligned} &-k^2 D a_n(k,t) - \frac{da_n(k,t)}{dt} \\ &= \int_{r=0}^{\infty} BI(t) \left[e^{-g^2 r^2} \int_{\ell=0}^{\infty} a_{n-1}(\ell,t) J_0(lr) l dl \right] J_0(kr) r dr \\ &= \int_{l=0}^{\infty} BI(t) a_{n-1}(l,t) \left[\int_{r=0}^{\infty} e^{-g^2 r^2} J_0(kr) J_0(lr) r dr \right] \\ &\times l dl = b_{n-1}(k,t) \end{aligned} \tag{7}$$

where

$$b_{n-1}(k,t) = \frac{BI(t)}{2g^2} \int_{l=0}^{\infty} a_{n-1}(l,t) e^{-\frac{k^2+l^2}{4g^2}} I_0\left(\frac{kl}{2g^2}\right) l dl \tag{8}$$

Evaluation of the inner integral in Eq. (7) is per Gradshteyn and Ryzhik 6-633.2 [13]. The right-hand side of Eq. (7) is thus an explicit function of t, namely through the known coefficients $a_{n-1}(k,t)$ comprising the previous term. The inhomogeneous first-order differential equation can be solved explicitly [14] and, if the initial condition is taken to be that $c = 1$ at $t = 0$, then we obtain

$$a_n(k,t) = e^{-k^2 Dt} \int_{t'=0}^{t} e^{k^2 Dt'} b_{n-1}(k,t') dt' \tag{9}$$

In the more general case, a distribution of diffusion coefficients D_i having fractions f_i, respectively, will be observed. In either case, we may write

$$s(k,t) = \sum_i f_i e^{-k^2 D_i t} \tag{10}$$

Then Eq. (8) can be re-written as a convolution

$$a_n(k,t) = \int_{t'=0}^{t} s(k, t-t') b_n(k,t') dt' = s(k) \otimes b(k) \tag{11}$$

The preceding equation allows the fluorophore distribution function c to be evaluated for any beam intensity varying arbitrarily with time and for any diffusion constant distribution. For computational purposes, the integration indicated in Eq. (8) can be conveniently accomplished by multiplying a vector containing the a_{n-1} by a suitable matrix. A Fast Fourier Transform-based convolution allows Eqs. (9) and (11) to be evaluated efficiently and this overall strategy affords a particularly efficient approach to describing diffusive behavior in kinetically heterogenous systems. Depending upon the diffusion constant, probe bleaching rate and extent of bleaching in the bleaching pulse, various number of terms in Eq. (4) may be needed to achieve satisfactory series convergence. We typically begin with eight such terms and adjust this number as needed. Once the fluorophore concentration is evaluated, the experimental fluorescence signal $F(t)$ is easily calculated as

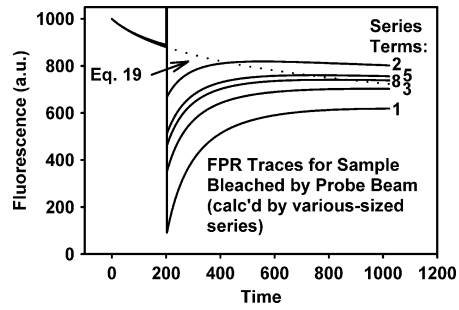

Fig. 1. FPR traces for a sample bleached by a Gaussian probe beam. $r_0 = 1$, $D = 0.002 r_0^2/pt$, $b = 0.002/pt$, $K = 1.6$. Various number of terms have been used in the series solution. It is evident that at least five terms are needed to represent the actual recovery. The dotted line, calculated from Eq. (19) which corresponds effectively to a one-term series solution, represents the level to which a fully mobile fluorophore would recover.

$$F(t) = \frac{F_0}{2g^2} \int_{r=0}^{\infty} e^{-g^2 r^2} I(t) c(r,t) r dr \tag{12}$$

Figure 1 shows a FPR trace for a sample bleached by the probe beam as calculated by the process just described. The diffusion constant is $0.002 r_0^2/pt$. A series of eight terms was used and the Figure shows the recovery trace obtained as various numbers of terms are retained. The extent of probe bleaching observed here, $0.002/pt$, represents near to the maximum amount which would be of interest as does the amount of bleaching in the pulse, approximately 50%. It is clear that at least five terms are needed to model this situation even approximately and all eight terms can profitably be used. Such simulations make clear that, whenever data include a substantial amount of probe bleaching, analysis using a first-order approximation is inadequate. The figure also includes a baseline, calculated via Eq. (19) developed in Appendix 1, which suggests, very approximately, the level to which fluorescence of a fully mobile species would recover after a bleaching pulse. A more accurate baseline can be calculated by evaluating Eq. (12) for a sufficient number of terms and omitting the bleaching pulse so that only bleaching from the constant-intensity probe beam is considered.

In general, we have found that either the Bessel-Fourier transform approach just described or a direct simulation approach outlined subsequently are most practical for analysis of actual cellular data since both methods accommodate large amount of bleaching by either probe or bleaching pulse and such large degrees of bleaching are common in cellular experiments. However, if extents of bleaching by the probe and pulse are both small, then a derivation shown in Appendix 1 provides an analytical expression for the shape of the fluorescence baseline in the absence of a bleaching pulse, as well as for recovery after a bleach.

Approach 2: Direct simulation of recovery kinetics given arbitrary extents of bleaching and arbitrary beam profiles.

Analytical expressions like those described above can be valuable aids to understanding the underlying physical reality of a given photobleaching experiment and for analysis of particular types of photobleaching data. However, such solutions can be quite complex and each is devised for a particular beam profile. Thus, we found direct finite-difference solution of the coupled difusion and bleaching equation, i.e. Eq. (1) for radial coordinates, useful in data analysis. An optimized numerical solution of this equation in various coordinate systems [12] was used to simulate the time-evolution of fluorescence recovery kinetics within a special-purpose Marquardt non-linear fitting program. A key component of this analysis is that the time increments between successive evaluations of concentration profiles are allowed to vary in proportion to square of the spot size divided by the current diffusion coefficient. This permits the calculation to proceed with the maximum speed consistent with stability of the numerical solution. This process allows fluorescence traces obtained in spot, fringe and other FPR bleaching geometries, each involving arbitrary extents of probe bleaching to be conveniently analyzed. For instance, we have previously applied this approach to analysis of interference fringe FPR data obtained using total internal reflection illumination [4].

RESULTS AND DISCUSSION

Even Small Amounts of Sample Bleaching in the Probe Beam Can Invalidate Diffusion Parameters Obtained by Conventional FPR Methods

Figure 2 simulates a spot photobleaching recovery trace as typically recorded for a membrane protein on a single cell. This trace illustrates the consequences of increasing FPR probe beam intensity in an effort to increase fluorescence signal. Equation (12) was used to simulate behavior of a protein with a diffusion coefficient of 1×10^{-10} cm^2 s^{-1} and a mobility (M) of 100% in a 1 μm probe beam which bleaches at a rate of 0.001 s^{-1}. As seen in the figure, these data *appear* to be more-or-less satisfactorily fitted by a conventional $(1+t/t_{1/2})^{-1}$ recovery kinetics model [1]. However, the recovered parameters bear little relation to those which generated the data. The diffusion coefficient is recovered as 1.7×10^{-10} cm^2 s^{-1} or 70% too high while the mobility is estimated as only 75%, that is, 25% too low. Similar difficulties also arise with data obtained fringe photobleaching where bleaching by the probe beam occurs. One must now ask what factors invalidate the diffusion parameters obtained.

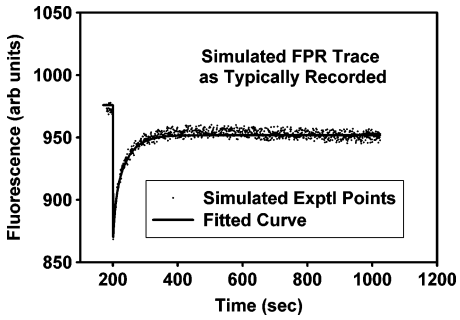

Fig. 2. Simulated photobleaching recovery data as typically recorded for a single cell. The sample has been exposed to the probe beam for a substantial time before data are obtained. Naive analysis of these data (smooth curve) yields grossly inaccurate diffusion parameters (see text).

Obtaining Accurate Diffusion Parameter from Spot FPR Requires Either That the Probe Beam Intensity be Very Low or That Data be Obtained from the Instant of Cell Exposure to the Probe Beam

The reason for the previously described discrepancy becomes apparent upon inspection of Fig. 3. This plot shows the full theoretical curve giving rise to the simulated experimental data in Fig. 2. As is typical in such experiments, the sample has been exposed to the probe beam for a substantial but indeterminate time before experimental data are recorded and thus the rate and extent of sample bleaching in the probe beam are never apparent. It is the magnitude of this on-going bleaching which invalidates the calculated results. Naturally, such bleaching can be avoided by use of extremely low probe beam intensities. However, such intensities rarely yield satisfactory data, especially with sparsely expressed membrane proteins. However, if data are taken from the instant of cell encounter with the probe beam (Fig. 4) and analyzed properly, then the parent diffusion parameters can be

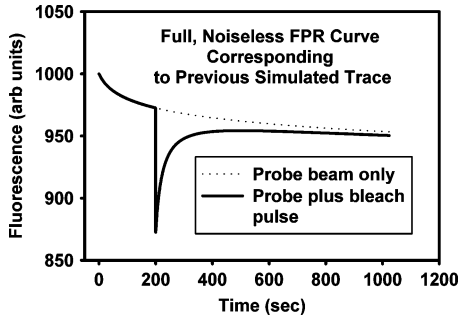

Fig. 3. Full theoretical curve (Eq. (12)) corresponding to the simulated experimental curve in Fig. 2. The substantial sample bleaching in the probe beam is only apparent when data are acquired from the beginning of cell exposure to this beam.

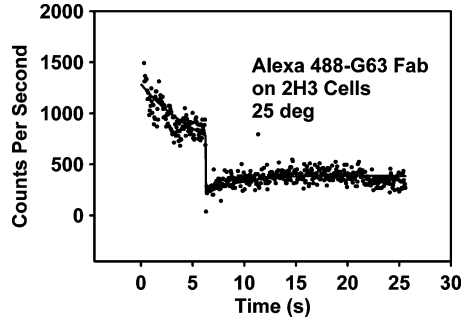

Fig. 5. Measurement by HPI-FPR of lateral diffusion of the sparsely expressed MAFA protein on 2H3 cells. Previously, measurement of this diffusion by conventional spot FPR proved impossible and interference fringe methods had to be employed.

accurately recovered. This type of data, which includes points beginning at the initial cell exposure to the probe beam, can only be obtained using some special technique to identify, align and focus on the cell. We use transmitted light to identify cells and a low-power 635 nm diode laser co-linear with the argon laser probe beam to align cells in the laser beam and to focus the beam on one or another membrane. This figure also shows why data analysis must be based on a model properly describing probe bleaching. Such bleaching causes sample fluorescence to decrease with time in a complicated logarithmic fashion (Eq. (19)) so that the "baseline" to which fluorescence recovers never becomes level or even linear.

HPI-FPR Measurements Yield Diffusion Parameters for VFP-Species with Precision Improved Over Conventional Spot FPR Methods

Figure 5 compares conventional and high probe intensity fluorescence recovery curves for GFP-LHR expressed on CHO cells. The probe intensity used in the conventional trace was selected to give no *apparent* bleaching over several recovery half times while the probe beam in the HPI-FPR experiment caused approximately 50% bleaching over this period. Analysis of the traces gives diffusion parameters agreeing well with one another, yielding values of $(5.6 \pm 6.2) \times 10^{-10}$ and $(9.2 \pm 5.9) \times 10^{-10}$ cm^2 s^{-1} and mobilities of (53 ± 17) and (47 ± 42)% for the conventional and HPI-FPR traces with $n = 67$ and $n = 26$, respectively. These measurements demonstrate that the experimental and data analysis techniques described previously satisfactorily deal with large extents of probe bleaching. Thus much larger signals can be obtained using HPI-FPR methods, in this instance, approximately 7-fold larger than that obtained in the conventional experiment. The statistical uncertainty in measured diffusion parameters is thus improved 2.6-fold by the HPI-FPR approach, as is also seen by comparison of the estimates of uncertainties in the fitted parameters yielded by the non-linear curve fitting procedures (data not shown). We have also applied HPI-FPR methods to measuring mobilities of a number of other VFP-membrane proteins, including GFP-gonadotropin releasing hormone receptor, GFP-erbB1 and YFP-erbB2, all expressed on CHO cells (data not shown).

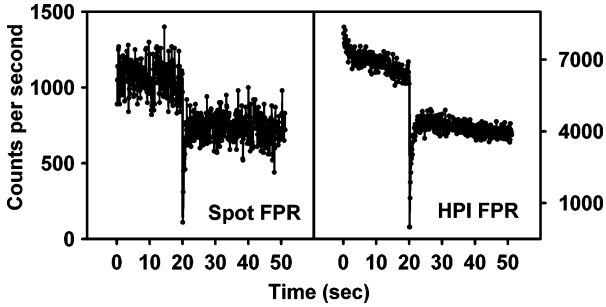

Fig. 4. Comparison of conventional spot FPR and HPI-FPR measurements of GFP-LHR lateral diffusion on CHO cells at 25°C. The HPI measurements affords 7-fold increased signal and hence 2.6-fold improved statistical precision.

HPI-FPR is Applicable to Membrane Proteins Bearing Antibody or Hormone Labels as Well as to VFP Fusion Proteins

The enhanced FPR method described above is applicable to any fluorescent cell surface species and will be useful whenever receptor expression is sparse and/or when cells exhibit *any* type of cytoplasmic fluorescence. One example of such a situation is the Mast Cell Function-Associated Antigen (MAFA) regulatory protein [7] of

2H3 cells which occurs in only 20,000 copies per cell. Fig. 5 shows successful measurement of MAFA diffusion on these cells by means of HPI spot photobleaching measurements using Alexa 488-G63 MAFA-specific Fab probe. Previous attempts to measure this diffusion by conventional spot FPR proved unsuccessful owing to low fluorescence signals. Analysis of the HPI data shown yields a diffusion constant of $(0.4 \pm 0.2) \times 10^{-10}$ cm^2 s^{-1} and a fractional mobility of $(68 \pm 23)\%$ for $n = 3$. These values differ somewhat from previously published results [7] determined by interference fringe methods, namely $(1.1 \pm 0.4) \times 10^{-10}$ cm^2 s^{-1} and $(31 \pm 7)\%$ for $n = 8$. Given the extremely low expression level of MAFA, and correspondingly low membrane fluorescence, it seems likely that this discrepancy arises in part from cytoplasmic fluorescent species, which unavoidably contribute to interference fringe photobleaching, but which are rejected by the confocal aperture used in HPI-FPR. Moreover, we have noted substantial cell-to-cell variability in FPR measurements on MAFA. This may arise from statistical fluctuations in the number and environment of the small number, perhaps 50, of MAFA molecules examined in any single spot photobleaching experiment. Other instances, not included here, of HPI-FPR measurements of mobilities of membrane proteins bearing antibody or hormone labels include TRITC-labeled human chorionic gonadotropin bound to LHR expressed on 293 cells and Type I Fcε receptor-bound Cy3-IgE on 2H3 cells.

CONCLUSIONS

We report here an advance in fluorescence photobleaching recovery techniques for measuring membrane molecule diffusion on living cells. This technique addresses problems arising from low levels of receptor expression in the presence of fluorescent cytoplasmic species. Hence it is particularly well-suited to examining membrane dynamics of VFP-fusion proteins. Other investigators, for example [11], have considered effects of probe bleaching on photobleaching recovery measurements, but we present here the first procedure for dealing with laser intensities which vary arbitrarily over time and for analyzing data obtained high extents of bleaching by either the probe beam or bleaching pulse. HPI-FPR maintains the confocality of conventional spot measurements but allows many-fold enhanced signals to be obtained. An important contribution of improved precision in such measurements is the possible identification of cell-to-cell variation in biophysical parameters currently obscured by the poor reproducibility of diffusion data. Moreover, the techniques presented for HPI-FPR data analysis are equally applicable to continuous photobleaching experiments and make possible straightforward analysis of such measurements where excitation intensity varies continuously over time.

APPENDIX 1: SMALL EXTENTS OF PROBE AND PULSE BLEACHING IN A GAUSSIAN SPOT

Consider a sample examined in a probe beam of constant peak intensity I_p where the ongoing rate of bleaching is small, i.e. that $BI_p \ll 1$, and where a brief pulse of high peak intensity I_b and duration Δt quickly bleaches a small "crater" in the sample. We can without loss of generality replace c with $1-c_b$ where $c_b = c_b(r, t)$ represents the fraction of irreversible photobleaching at any instant. Then, after the conclusion of the bleaching pulse and since the extent of bleaching is small, Eq. (2) becomes

$$-D\nabla^2 c_b + \frac{\partial c_b}{\partial t} = Be^{-g^2 r^2} I_p (1 - c_b) \tag{13}$$

We insist that c_b and $\exp(-g^2 r^2)$ can both be represented by Bessel-Fourier expansions.

$$\begin{aligned} c_b(r, t) &= \int_{k=0}^{\infty} a(k, t) J_0(kr) k dk \\ e^{-g^2 r^2} &= \int_{k=0}^{\infty} \left(\frac{1}{2g^2} e^{-k^2/4g^2} \right) J_0(kr) k dk \end{aligned} \tag{14}$$

Inserting these expressions into Eq. (3) we obtain

$$Dk^2 a(k, t) + \frac{da(k, t)}{dt} = \frac{BI_p}{2g^2} e^{-k^2/4g^2} \tag{15}$$

Then, observing that $a_k(0) = 0$, the solution of Eq. (5) can be written by inspection as

$$a(k, t) = \frac{BI_p}{2Dg^2 k^2} e^{-k^2/4g^2} \left(1 - e^{-k^2 Dt}\right) \tag{16}$$

Equation (16) effectively represents the Bessel-Fourier expansion of the first term of Eq. (4). While an analytical expression for the actual fluorophore distribution can, with sufficient effort, be obtained, we actually require only the time-dependent normalized fluorescence depletion *signal* $\Delta F = F(0) - F(t)$ which is given by

$$\begin{aligned} \Delta F / F(0) &= 2g^2 \int_{r=0}^{\infty} c_b(r, t) e^{-g^2 r^2} I_p \, r dr \\ &= \frac{BI_p}{D} \int_{r=0}^{\infty} e^{-g^2 r^2} \left(\int_{k=0}^{\infty} \frac{1}{k^2} e^{-k^2/4g^2} \right. \\ &\quad \left. \times \left(1 - e^{-k^2 Dt}\right) J_0(kr) k dk \right) r dr \\ &= \frac{BI_p}{2g^2 D} \int_{k=0}^{\infty} e^{-k^2/2g^2} \left(1 - e^{-k^2 Dt}\right) \frac{dk}{k} \end{aligned} \tag{17}$$

Now, we substitute z for $k^2/2g^2$ and t' for $2g^2Dt$ to obtain

$$\begin{aligned}\Delta F/F(0) &= \frac{BI_p}{4g^2D}\sum_{n=1}^{\infty}\frac{(-1)^{n-1}t'^n}{n!}\int_{z=0}^{\infty}z^{n-1}e^{-z}dz \\ &= \frac{BI_p}{4g^2D}\sum_{n=1}^{\infty}\frac{(-1)^{n-1}t'^n}{n} \\ &= \frac{BI_p}{4g^2D}\ell n\left(1+t'\right)\end{aligned} \tag{18}$$

We can replace g^2 with $2/r_0^2$ and t' with $t/t_{1/2}$ to obtain.

$$\Delta F/F(0) = \frac{BI_pt_{1/2}}{2}\ell n\left(1+t/t_{1/2}\right) \tag{19}$$

Equation (19) provides a convenient closed-form approximation of the evolution of fluorescence signal during bleaching from the probe beam and, in Fig. 5, this approximate baseline is shown as a dotted line. The amount of bleaching in this example is too high for Eq. (19) to apply quantitatively, since eight terms in Eq. (4) were needed to represent the recovery after the bleaching pulse and Eq. (19) is derived from only the first such term. Nonetheless, the plot makes clear that the baseline to which fluorescence recovers in the presence of bleaching by the probe beam never becomes flat or even linear. Hence, data analysis needs to explicitly deal with probe bleaching if diffusion parameters are to be recovered accurately.

Because the extent of bleaching by both probe and pulse is assumed to be small, the recovery of fluorescence signal after a brief bleaching pulse of intensity I_b and duration Δt and occurring at a time t_b after initial exposure of the sample to light, can, as a first-order approximation, be calculated independently. For derivation of this recovery, see, for example, Axelrod *et al.* [1]. The final result becomes

$$\begin{aligned}F/F(0) &= 1-\frac{BI_pt_{1/2}}{2}\ell n\left(1+t/t_{1/2}\right) \quad (t<t_b) \\ &= 1-\frac{BI_pt_{1/2}}{2}\ell n\left(1+t/t_{1/2}\right) \\ &\quad -\frac{BI_b\Delta t}{2}\frac{1}{1+(t-t_b)/t_{1/2}} \quad (t\geq t_b)\end{aligned} \tag{20}$$

APPENDIX 2: SMALL EXTENTS OF PROBE AND PULSE BLEACHING IN A UNIFORM CIRCULAR SPOT

In certain situations, for example when photobleaching an extended spot in a confocal microscope, a circular region of radius r_0 may be illuminated effectively uniformly with light of intensity I_p. This allows a approximate solution of the diffusion equation using Laplace transforms by solving the diffusion equations inside and outside the spot separately and then insisting the fluorophore concentration be continuous across the spot boundary. In fact, only the fluorophore concentration inside the spot is required as only from there does fluorescence signal arise. The key elements in this approach are demonstrated in Ozişik's examples 8–1 and 7–22 [15]. We begin with separate equations inside and outside the spot, designating c_1 and c_2 the fluorophore concentrations inside and outside, respectively. For convenience we denote bleaching rate constant BI_p by the symbol h

$$\begin{aligned}D\nabla^2c_1(r,t)-hc_1(r,t) &= \frac{dc_1(r,t)}{dt} \quad (0\leq r\leq b) \\ D\nabla^2c_2(r,t) &= \frac{dc_2(r,t)}{dt} \quad (b\leq r<\infty)\end{aligned} \tag{21}$$

We apply the Laplace transform with respect to time, insist that both c_1 and c_2 are everywhere 1 at $t=0$ and denote the transform variable by s and the transforms of c_1 and c_2 by θ_1 and θ_2, respectively. There results

$$\begin{aligned}D\nabla^2\theta_1-(h+s)\theta_1 &= 0 \quad (0\leq r<r_0) \\ D\nabla^2\theta_2-s\theta_2 &= 0 \quad (r_0<r<\infty)\end{aligned} \tag{22}$$

The solutions of Eq. set (22) are linear combinations of modified Bessel functions I_0 and K_0. Since θ_1 is finite for $r=0$, θ_1 contains no K_0. Likewise, since θ_2 is unity at $r=\infty$ for all t, θ_2 contains no I_0. It is convenient to denote $(s/D)^{1/2}$ by m and $((s+h)/D)^{1/2}$ by n. Then

$$\begin{aligned}\theta_1 &= UI_0(nr) \\ \theta_2 &= VK_0(mr)\end{aligned} \tag{23}$$

where U and V are constants. Insisting that θ_1 and θ_2, and their first derivatives as well, agree at $r=r_0$ for all t allows evaluation of U and V and hence of θ_1 and θ_2.

$$\begin{aligned}\theta_1 &= \frac{1}{s+h}+\frac{\left(\frac{1}{s}-\frac{1}{s+h}\right)[mK_1(mr_0)I_0(nr)]}{mI_0(nr_0)K_1(mr_0)+nI_1(nr_0)K_0(mr_0)}; \\ \theta_2 &= \frac{1}{s}-\frac{\left(\frac{1}{s}-\frac{1}{s+h}\right)[mK_0(mr_0)I_1(nr)]}{mI_0(nr_0)K_1(mr_0)+nI_1(nr_0)K_0(mr_0)}\end{aligned} \tag{24}$$

Inversion of the Laplace transform involves use of asymptotic expansions for the modified Bessel functions and their derivatives valid for large s and, hence, for small times t. These expansions can be found in Abramowitz and Stegun sections 9.7.1–9.7.4 [16] and yield the Laplace transform as a series of terms of the form $e^{-\sqrt{s}}/s^{n/2}$. These terms can be inverted to obtain a series solution valid for $r\neq0$ and for short times t. We present here only the lowest-

order term exhibiting coupling of diffusion and bleaching by the probe beam.

$$c_1 = e^{-ht}\left(1 - \frac{h}{4D}\sqrt{\frac{r_0}{r}}\left\{2(r_0 - r)\sqrt{\frac{Dt}{\pi}}e^{-(r_0 - r)^2/4Dt}\right.\right.$$
$$\left.\left. + \left[(r_0 - r)^2 + 2Dt\right] erfc\frac{r_0 - r}{2\sqrt{Dt}}\right\} + \cdots\right) \quad (0 < r \le r_0)$$
$$c_2 = 1 - \frac{h}{4D}\sqrt{\frac{r_0}{r}}\left\{-2(r - r_0)\sqrt{\frac{Dt}{\pi}}e^{-(r - r_0)^2/4Dt}\right.$$
$$\left. + \left[(r - r_0)^2 + 2Dt\right] erfc\frac{r - r_0}{2\sqrt{Dt}}\right\} + \cdots \quad (r_0 \le r < \infty) \tag{25}$$

However, since our interest actually lies only in the fluorescence signal, we can return to Eq. (4) and integrate across the illuminated area to obtain the average Laplace transform, proportional to the total fluorescence signal.

$$\langle\theta_1\rangle = \frac{1}{s + h} + \frac{2}{nb}\frac{(\frac{1}{s} - \frac{1}{s+h})\,[mK_1(mb)I_1(nb)]}{mI_0(nb)K_1(mb) + nI_1(nb)K_0(mb)} \tag{26}$$

Again using series expansion of the modified Bessel functions and inverting, we find that the fluorescence signal can be represented as

$$F = F_0 e^{-ht}\left(1 + \frac{4h}{3r_0}\sqrt{\frac{Dt^3}{\pi}} + \cdots\right) \tag{27}$$

Figure 6 shows the evolution of fluorescence from a uniformly illuminated region experiencing coupled bleaching and diffusion as described in Eq. (25) for a sample with $D = 0.02r_0^2/pt$ and $h = 0.02/pt$. The coupling of diffusion and bleaching is clear from the evolution over time of the shape of the bleached region which is initially flat but soon becomes a rounded depression. The actual fluorescence signal for $D = 0.02$ and $D = 0$ is plotted in the inset of Fig. 6. As is the case for a Gaussian spot, a plot of the fluorescence versus time shows a steeper initial portion and then a decreasing negative slope as diffusion into the bleached area becomes more significant. It is clear that the shape of the fluorescence baseline, in the absence of a bleaching pulse, will continue to evolve over time and so must be explicitly incorporated in analysis of FPR data accompanied by any noticeable amount of bleaching by the probe beam. One should note that this series treatment is only an approximation valid for short times and so does not itself provide a closed-form function suitable for projecting an extended fluorescence baseline in the absence of a bleaching pulse. For this purpose, numerical solution, as described above, of the differential equation describing coupled beaching and diffusion is necessary.

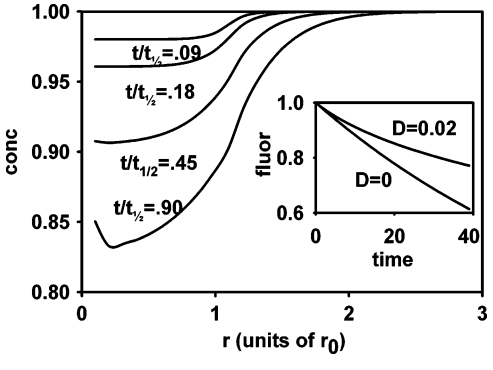

Fig. 6. Concentration profiles for a sample continuously bleached by a uniform circular probe beam. The inset shows how decay of sample fluorescence during observation in the presence and absence of diffusion.

ACKNOWLEDGMENTS

The Authors are grateful to Prof Professor Israel Pecht, Weizmann Institute of Science, Rehovot, Israel, for providing the MAFA-specific mAb G63. This work was supported in part by NSF grants MCB-0315798 and DBI-0138322 to BGB, by NIH grant HD23236 to DAR and by a postdoctoral fellowship to GCL by the Consejo Nacional de Ciencia y Tecnología (CONACYT), Mexico.

REFERENCES

1. D. Axelrod, D. E. Koppel, J. Schlessinger, E. Elson, and W. W. Webb (1976). Mobility measurement by analysis of fluorescence photobleaching recovery kinetics. *Biophys. J.* **16**, 1055–1069.
2. H. M. Munnelly, D. A. Roess, W. F. Wade, and B. G. Barisas (1998). Interferometric fringe fluorescence photobleaching recovery interrogates entire cell surfaces. *Biophys. J.* **75**, 1131–1138.
3. D. Axelrod, T. P. Burghardt, and N. L. Thompson (1984). Total internal reflection fluorescence. *Annu. Rev. Biophy. Bioeng.* **13**, 247–268.
4. B. G. Barisas, D. A. Roess, G. C. d. León, and G. M. Hagen (2004). Lateral diffusion measurements on genetically-introduced fluorescent proteins. *SPIE Proc.* **5329**, 44–53.
5. H. Schmidt, E. B. Brown, B. Schwaller, and J. Eilers (2003). Diffusional mobility of parvalbumin in spiny dendrites of cerebellar purkinje neurons quantified by fluorescence recovery after photobleaching. *Biophys. J.* **84**, 2599–2608.
6. R. D. Horvat, S. Nelson, C. M. Clay, B. G. Barisas, and D. A. Roess (1999). Intrinsically fluorescent luteinizing hormone receptor demonstrates hormone-driven aggregation. *Biochem. Biophys. Res. Commun.* **256**, 382–385.
7. J. Song, G. Hagen, D. A. Roess, I. Pecht, and B. G. Barisas (2002). Time-resolved phorescence anisotropy studies of the mast cell function-associated antigen and its interactions with the Type I Fcε receptor. *Biochemistry* **41**, 880–889.
8. M. Scholz, K. Schulten, and R. Peters (1985). Single-cell flux measurement by continuous fluorescence microphotolysis. *Eur. Biophys. J.* **13**, 37–44.

9. X. Ferrieres, A. Lopez, A. Altibelli, L. Dupou-Cezanne, J. L. Lagouanelle, and J. F. Tocanne (1989). Continuous fluorescence microphotolysis of anthracene-labeled phospholipids in membranes. Theoretical approach of the simultaneous determination of their photodimerization and lateral diffusion rates. *Biophys. J.* **55**, 1081–1091.
10. M. Wachsmuth, T. Weidemann, G. Muller, U. W. Hoffmann-Rohrer, T. A. Knoch, W. Waldeck, and J. Langowski (2003). Analyzing intracellular binding and diffusion with continuous fluorescence photobleaching. *Biophys. J.* **84**, 3353–3363.
11. E. Endress, S. Weigelt, G. Reents, and T. M. Bayerl (2005). Derivation of a closed form analytical expression for fluorescence recovery after photo bleaching in the case of continuous bleaching during read out. *Eur. Phys. J. E. Soft. Matter* **16**, 81–87.
12. S. J. Farlow (1982). *Partial Differential Equations for Scientists and Engineers*. Dover Publications, New York, 414 pp.
13. I. S. Gradshteyn and I. M. Ryzhik (1965). *Table of Integrals, Series, and Products*. Jeffrey A, Translator. Academic Press, New York, 1086 pp.
14. W. Kaplan (1958). *Ordinary Differential Equations*. Addison-Wesley, Reading, MA, xv+534 pp.
15. M. N. Özisik (1980). *Heat Conduction*. Wiley, New York, 687 pp.
16. M. Abramowitz and I. A. Stegun (1968). *Handbook of Mathematical Functions*. Dover Publications, New York.